Multi-Channel Differential Synchronous Demodulator for Linear Inductive Position Sensor

Jun XUE [1], Dezhi WANG [2]

[1] Dept. of Computer and Information Engineering, Wuhan Railway Vocational College of Technology, Wuhan, China
[2] Dept. of Microelectronics, Hubei University, Wuhan, China

xuejun@wru.edu.cn, dzjcwang@hubu.edu.cn

Submitted May 30, 2024 / Accepted August 8, 2024 / Online first September 30, 2024

Abstract. *A multi-channel differential synchronous demodulator is proposed for third harmonics suppression in three-phase receiving coils based linear inductive position sensor, which is realized by taking envelope differences of every two induced signals on three-phase receiving coils as differential signals. The proposed demodulator includes a differential synchronous envelope detector (DSED), and a time division MUX (TDM). By using the DSED, the envelope differences are synchronously demodulated as differential signals. The TDM including a multi-channel selector, a MUX and a voltage follower, is used for independently outputting the corresponding differential signals for linear position calculation. The proposed demodulator was designed in a 180 nm CMOS process and verified by Spectre simulator. Simulation results show third harmonics of differential signals are improved by 17.4 dB, indicating the proposed demodulator could be a candidate for designing the high performance analog front-end of inductive position sensor.*

Keywords

Inductive position sensor, multi-channel, differential synchronous demodulator, third harmonics noise

1. Introduction

Inductive position sensor (IPS) mainly includes an exciting coil, a rotor, several receiving coils and a signal conditioning chip. The induced voltages on receiving coils are similar to the process of electromagnetic coupling in near-field communication [1], and their values vary with rotor's position. Thus, the position of rotor could be calculated based on the induced voltages on receiving coils. Compared with hall position sensor, IPS is more popular for automobiles, electric motors and robotics as its advantages of low cost, high accurate and anti-electromagnetic interference [2–4]. A classical method utilizes quadrature receiving coils and arc tangent operation to solve rotor's position, whereas arc tangent undergoes singularities at $\pi/2$ and $3\pi/2$ [5–8]. Using three-phase receiving coils based linear position calculation could avoid singularities and benefit higher computational efficiency, thus they are widely used in IPS [9]. A non-contact vertical inductive torque sensor proposed by Zhang, C. provided a method of three-phase receiving coils based linear position calculation, however, envelopes of induced signals used in the method undergo third harmonic [10]. Fortunately, envelope differences are immune to third harmonic and their properties are the same as envelopes. Thus, envelope differences based linear position calculation is a preferred method, and the related solutions are reported recently [11–13].

Analog front-end, including a demodulator, a variable gain amplifier (VGA) and an analog to digital convertor (ADC), is one of the most important modules in signal conditioning chip, in which the VGA and ADC act the same as traditional circuits in wireless transceiver [14], [15]. However, most works focus on the design of analog front-end in quadrature receiving coils based IPS [5–8], [16]. And, active demodulator [17], [18] or instrumentation amplifier [19], [20] are usually chosen to realize the demodulator for ultra-low DC offset, which are large noise and high cost. These methods are inadvisable as DC offset could not affect the linearity of analog front-end and it could be removed by post calibration.

Based on the above discussions, we propose a multi-channel differential synchronous demodulator used for three-phase receiving coils based linear inductive position sensor. The proposed demodulator consists of a DSED and a TDM, in which the TDM includes a multi-channel selector (MCS), a MUX and a voltage follower (VF). With the DSED, envelope differences of every two induced signals on three-phase receiving coils are synchronously demodulated as differential signals. The TDM is used for independently outputting the corresponding differential signals for linear position calculation. The advantages of this work are as follows. The proposed demodulator benefits simple structure, low cost and low noise, as digital circuits and passive filters are used and envelope differences are taken as differential signals. Moreover, an algorithm of channel switching is proposed for linear position calculation, which is realized by the MCS.

DOI: 10.13164/re.2024.0519

2. Theoretical Basis

Layout of a transmitting coil, a receiving coil and a rotor in an IPS is shown in Fig. 1. The rotor has three laminas, the receiving coil has six closed-loop frames and the adjacent frames are reversely wound.

When the transmitting coil is driven by an exciting signal $\sin(\omega_e t)$, the receiving coil would generate an induced voltage $A_m \sin(3\theta)\sin(\omega_e t)$, in which the U_1 equaling $A_m \sin(3\theta)$ is the envelope of induced voltage [21]. Supposing the angle of rotor is 0 when the rotor lies in the position as shown in Fig. 1, then U_1 equals 0 as the induced voltages of clockwise coil and counterclockwise coil are the same. If the rotor continues rotating in clockwise, U_1 varies by degrees as shown in Fig. 2 [22].

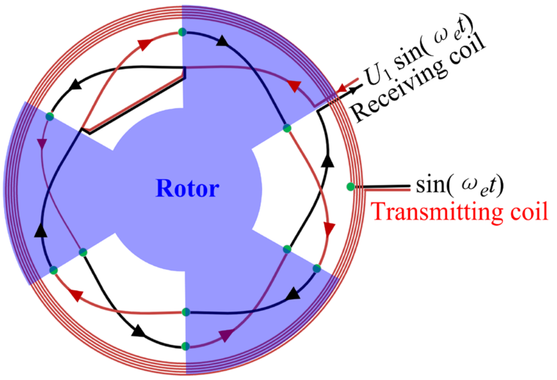

Fig. 1. Layout of a receiving coil, an exciting coil and a rotor in an IPS.

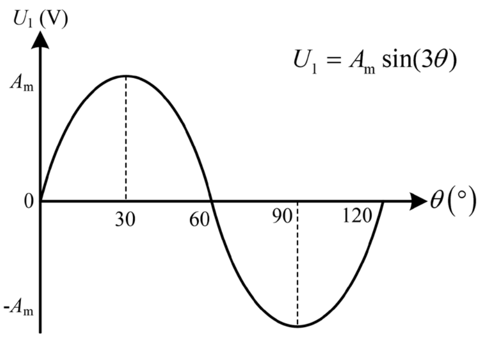

Fig. 2. The envelope of induced voltage on receiving coil.

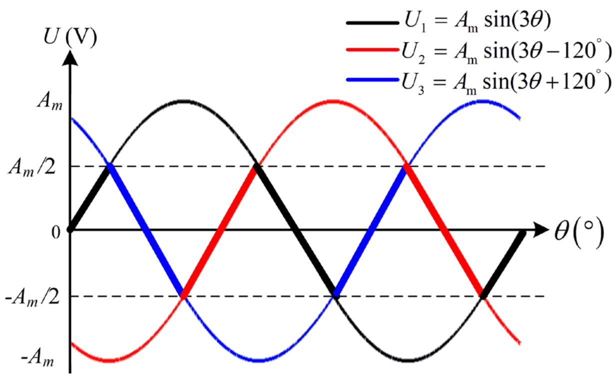

Fig. 3. The envelope of induced voltages on three-phase receiving coils.

Similarly, U_1, U_2 and U_3 are shown in Fig. 3 when three-phase receiving coils are wound with 120° apart from each other. The slope of $U_{1,2,3}$ has the minimum value when their values reach to the peak value, which means the position has the worst accuracy. Moreover, as the slope of curves between $-A_m/2$ and $A_m/2$ are approximately constant, the position of rotor could be calculated by regarding these curves as straight lines. Therefore, the position could be obtained once the values of U_1, U_2 and U_3 are detected, however U_1, U_2 and U_3 contain harmonics as given by (1), (2) and (3) simply because the exciting signal is not a purely sinusoidal field pattern:

$$U_1 = \sum_{i=0}^{\infty} A_i \sin\left[i(3\theta)\right], \tag{1}$$

$$U_2 = \sum_{i=0}^{\infty} A_i \sin\left[i(3\theta - 120°)\right], \tag{2}$$

$$U_3 = \sum_{i=0}^{\infty} A_i \sin\left[i(3\theta + 120°)\right]. \tag{3}$$

Then, the error of position calculation is as (4) assuming feeding wires connected to signal conditioning chip do not introduce additional errors and the intensity of various harmonics decreases with increasing order [11]:

$$\theta_{\text{error}} = -\frac{A_3}{A_1}\sin(12\theta). \tag{4}$$

On the other hand, envelope differences of every two of U_1, U_2 and U_3 are given by (5), (6) and (7)

$$Y_1 = U_1 - U_2 = \sum_{i=0}^{\infty} A_i \left\{\sin\left[i(3\theta)\right] - \sin\left[i(3\theta - 120°)\right]\right\}, \tag{5}$$

$$Y_2 = U_2 - U_3 = \sum_{i=0}^{\infty} A_i \left\{\sin\left[i(3\theta - 120°)\right] - \sin\left[i(3\theta + 120°)\right]\right\}, \tag{6}$$

$$Y_3 = U_3 - U_1 = \sum_{i=0}^{\infty} A_i \left\{\sin\left[i(3\theta + 120°)\right] - \sin\left[i(3\theta)\right]\right\}. \tag{7}$$

Obviously, waveforms of Y_1, Y_2 and Y_3 are similar to U_1, U_2 and U_3, and their values are 0 when i equals 3. Thus, envelope differences based linear position calculation is immune to third harmonic, and hence benefits high accurate according to (4). Moreover, as the sum of Y_1, Y_2 and Y_3 is 0, only two of them are needed to be detected for linearly position calculation.

3. Circuits Design

The proposed demodulator shown in Fig. 4 includes a DSED and a TDM, in which the TDM consists of a MUX, a MCS and a VF. The receiving coils of L_1, L_2 and L_3 are wound with 120° apart from each other, then the induced voltages on L_1, L_2 and L_3 are as (8), (9) and (10). The DSED is designed for demodulating the envelope differences

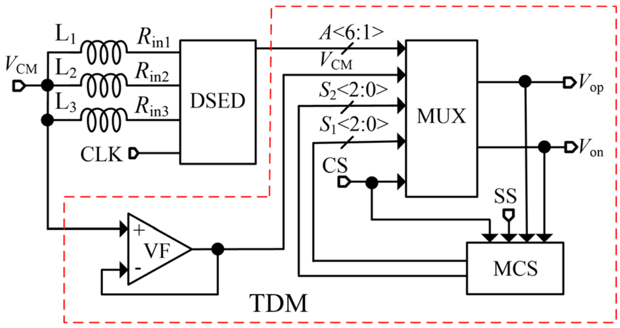

Fig. 4. The proposed multi-channel differential synchronous demodulator.

of every two of R_{in1}, R_{in2} and R_{in3} to differential signals. The TDM is proposed for independently outputting the differential signals in the corresponding channel, in which an algorithm of channel switching realized by MCS is proposed, so that the straight lines as depicted in Fig. 3 could be chosen for linear position calculation:

$$R_{\text{in1}} = V_{\text{CM}} + U_1 \sin(\omega_{\text{e}} t), \tag{8}$$

$$R_{\text{in2}} = V_{\text{CM}} + U_2 \sin(\omega_{\text{e}} t), \tag{9}$$

$$R_{\text{in3}} = V_{\text{CM}} + U_3 \sin(\omega_{\text{e}} t). \tag{10}$$

3.1 The Proposed DSED Circuit

The proposed DSED circuit is shown in Fig. 5. Envelope differences of every two of R_{in1}, R_{in2} and R_{in3} are synchronously demodulated as differential signals, namely, the differential pairs of A_1 and A_2, A_3 and A_4, A_5 and A_6.

Two phase non-overlapping clocks CLKP and CLKN are used for synchronous rectification, then S_1 and S_2, S_3 and S_4, S_5 and S_6 are the rectification results of R_{in1} and R_{in2}, R_{in2} and R_{in3}, R_{in3} and R_{in1}. A low pass filter (LPF) including resistor R_2 and capacitors of C_1 and C_2 is used to convert S<6:1> into envelopes A<6:1>. Hence, the values of A_1 minus A_2, A_3 minus A_4 and A_5 minus A_6 represent the values of Y_1, Y_2 and Y_3 respectively, which are immune to third harmonics according to (5), (6) and (7).

The signals S<6:1> undergo large spurs due to charge injection, large capacitor is preferred for reducing the spurs. MOS capacitor M_1 is utilized as it can realize large capacitance with small area. Besides, C_1 and C_2 are chosen as metal insulator metal (MIM) capacitor for reducing A<6:1>'s ripples. Two MIM capacitors are needed with top and bottom plates inversely connected to the circuit, in order to realize crossing symmetry for differential signal.

3.2 The Proposed TDM Circuit

As shown in Fig. 6, the proposed MUX used in TDM outputs A_1, A_3, A_5 to V_{op} and outputs A_2, A_4, A_6 to V_{on} in different channels, thus the differential signal of V_{op} minus V_{on} equals one of the Y_1, Y_2 and Y_3 in a channel. Based on the MUX circuit, Y_1 is output when S_2<2:0> and S_1<2:0> are "010" and "001", Y_2 is output when S_2<2:0> and S_1<2:0>

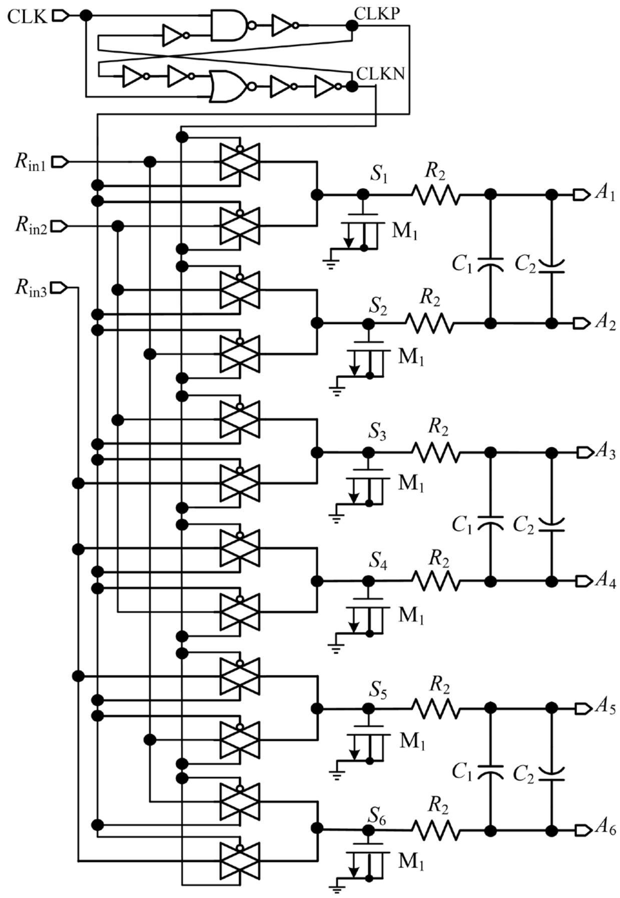

Fig. 5. The proposed DSED circuit.

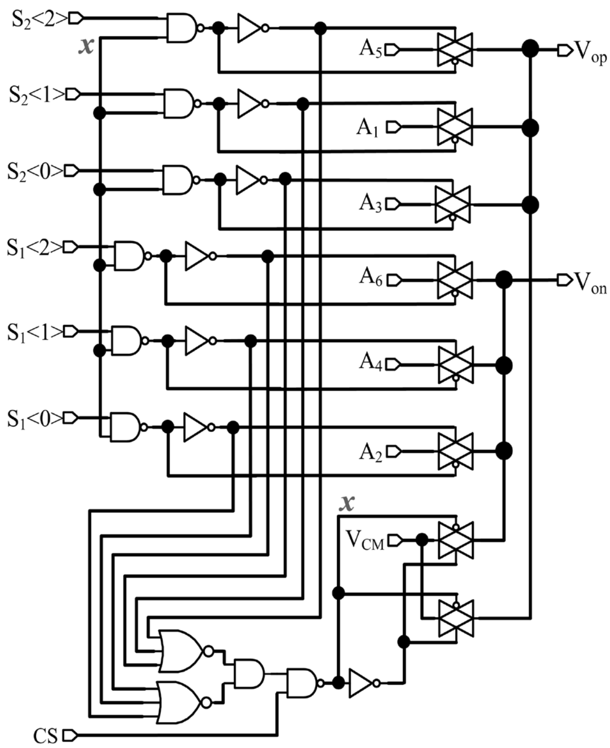

Fig. 6. The proposed MUX circuit.

are "001" and "010", and Y_3 is output when S_2<2:0> and S_1<2:0> are "100" and "100". The signal CS resets each channel to V_{CM} before S_2<2:0> and S_1<2:0> are set, in which the V_{CM} is connected to the common-mode voltage on three-phase receiving coils through a VF. Thus, each channel is independent of each other.

An algorithm of channel switching realized by MCS is explained based on Fig. 7. When $Y_1 > Y_2 > Y_3$, Y_2 would be selected for linear position calculation, and so do the other situations. Thus, the curves between $-A_1/2$ and $A_1/2$ could be selected for linear position calculation as shown in Fig. 7 by solid straight lines. In order to obtain the size relationship among Y_1, Y_2 and Y_3, two of the Y_1, Y_2 and Y_3 between $-A_1/2$ and $A_1/2$ should be detected as $Y_1 + Y_2 + Y_3 = 0$. We divide the waveforms into six regions as shown in Fig. 7, so that every region includes two of the Y_1, Y_2 and Y_3. For example, Y_3 and Y_2 are output in region II. Based on the proposed MUX circuit, we could further deduce the desired states of S_2<2:0> and S_1<2:0>, as shown at the bottom of Fig. 7. And, the complete state transition diagram of the proposed channel switching algorithm is given in Fig. 8.

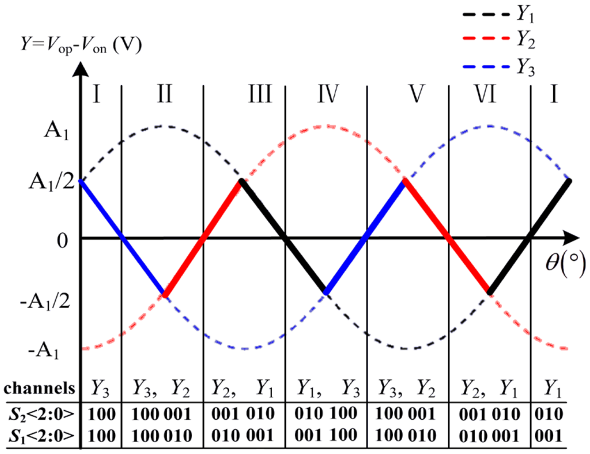

Fig. 7. The relationship between Y_1, Y_2, Y_3 and S_2<2:0>, S_1<2:0>.

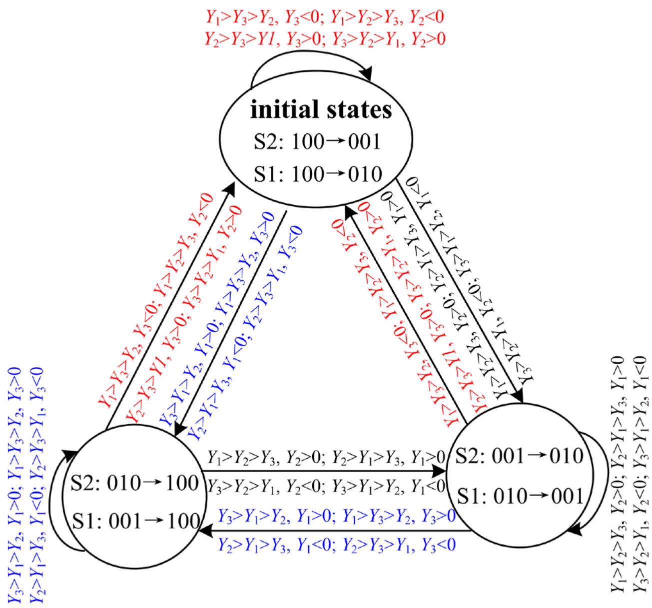

Fig. 8. The state transition diagram of the proposed algorithm.

4. Simulation Results and Discussions

The proposed multi-channel differential synchronous demodulator was designed in a 0.18 µm CMOS process, and verified by Spectre simulator. The system parameters for verifying the proposed demodulator are given in Tab. 1.

Simulation results of the process of demodulation is given by Fig. 8 when the envelopes of $R_{in1,2,3}$ are constant and CLK is synchronous with $R_{in1,2,3}$. As R_{in1} and R_{in2} are alternately transmitted to S_1 and S_2 when CLK is changed from “1” to “0”, S_1 and S_2 realize the rectification of R_{in1} and R_{in2}, and they are converted to DC levels A_1 and A_2 through the LPF. Thus the value of A_1 minus A_2 represents the envelope difference of R_{in1} and R_{in2}, namely, the size of Y_1. Moreover, A_3 minus A_4 and A_5 minus A_6 represent the sizes of Y_2 and Y_3, which are consistent with the envelope differences of every two of the $R_{in1,2,3}$ as shown in Fig. 9. Besides, the value of Y_1 is given in Fig. 10 when mismatch between CLK and $R_{in1,2,3}$ is set from 0 to 70 ns. The value of Y_1 is attenuated from 46 mV to nearly 0, which verifies the significance of synchronous demodulation.

When $R_{in1,2,3}$ last for more than one period of the $U_{1,2,3}$, simulation results about the function of TDM circuit are given in Fig. 11. The clocks CS and SS are used for channel’s resetting, sampling and detecting. During the time from t_1 to t_6, $Y_1 > Y_3 > Y_2$ and $Y_3 > 0$. At the time t_1, CS is “1”, S_2<2:0> and S_1<2:0> are “000” and “000”, SS is “0”, the voltages of V_{op} and V_{on} are reset to V_{CM}. At the time t_2, CS and SS are “0”, S_2<2:0> and S_1<2:0> are updated to “010” and “001” as $Y_1 > Y_3 > Y_2$ and $Y_3 > 0$, thus Y_1 is sampled. At the time t_3, SS is “1” while CS, S_2<2:0> and S_1<2:0> keep unchanged, then Y_1 is detected by the MCS. Similarly, Y_3 is detected during the time from t_4 to t_6 as S_2<2:0> and S_1<2:0> are “100” and “100”. Finally, Y_1, Y_2 and Y_3 are detected, and their values are used for linearly position calculation and the next update of S_2<2:0> and S_1<2:0>.

The completed waveforms of R_{in1} and R_{in2} in a period of envelope, the envelopes A_1 and A_2, and the envelope difference Y_1 are shown in Fig. 12. The amplitude and the third harmonic of $U_{1,2,3}$ are 22 mV or –33 dB and 11 mV or –39 dB. Simulation results show both A_1 and A_2 undergo third harmonic noise and large spurs caused by switching, however Y_1 is immune to the third harmonic and spurs.

The frequency spectrum of $A_{1,2}$ and Y_1 are given in Fig. 13. The third harmonic of $A_{1,2}$ and Y_1 are –64.4 dB and

Parameters		Values
$U_{1,2,3}$	frequency	250 Hz
	amplitude	22 mV
	third harmonic’s amplitude	11 mV
SS and CS [a]	frequency	500 kHz
	duty cycle	1/8
The frequency of $R_{in1,2,3}$ and CLK		3.3 MHz
V_{CM}		1.5 V
Phase mismatch between CLK and $R_{in1,2,3}$		0: 5 ns: 70 ns [b]

a) SS lags behind CS 1.625 µs; b) from 0 to 70 ns with 5 ns step

Tab. 1. System parameters of the proposed demodulator.

–82.2 dB, and the third harmonics of Y_2 and Y_3 not shown within the text are also much smaller than the third harmonics of $A_{1,2,3}$. These simulation results demonstrate the proposed demodulator is useful for the high performance analog front-end of three-phase receiving coils based linear IPS.

Comparisons of this work with the existing works are concluded in Tab. 2. The proposed demodulator is designed for three-phase receiving coils based IPS and it is realized by using digital circuits and passive filters. Thus, circuit's structure of the proposed demodulator is much simpler than the existing works, the noise is less than in the existing works, and the third harmonics are smaller than the references [5, 6, 8, 10].

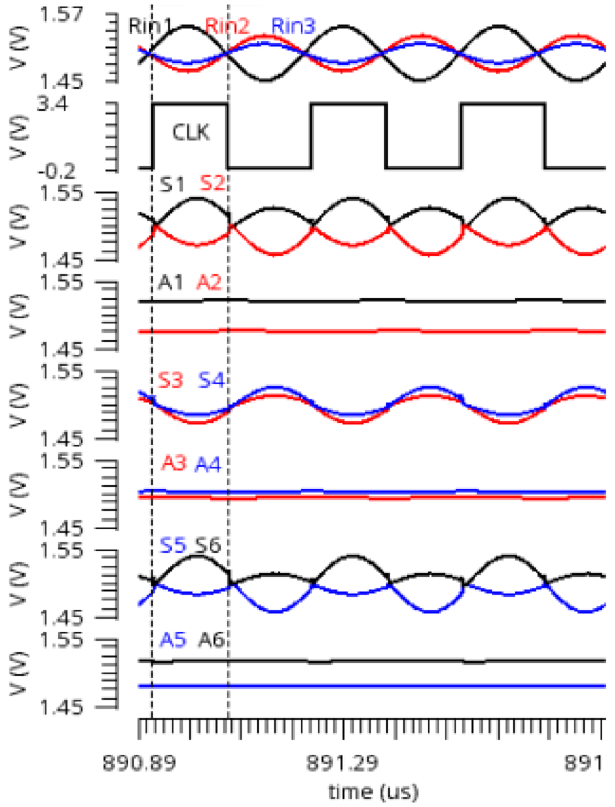

Fig. 9. Simulation results of the process of demodulation.

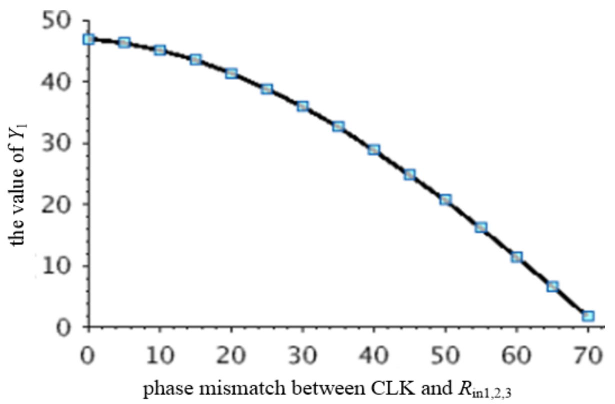

Fig. 10. Simulation results of Y_1's attenuation.

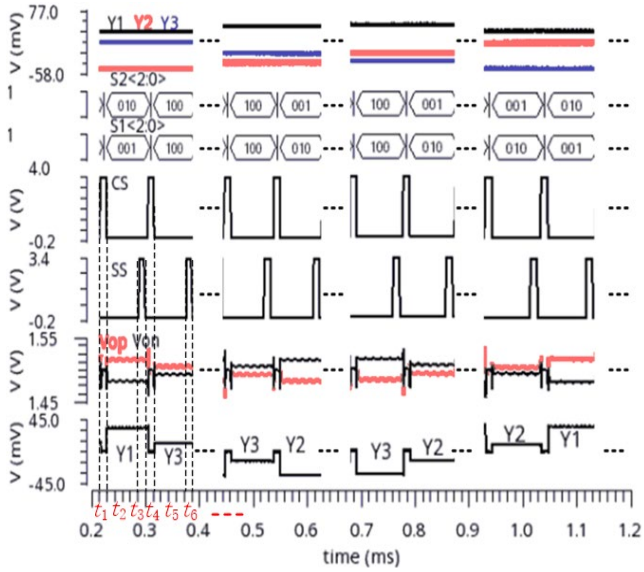

Fig. 11. Simulation results about the function of TDM circuit.

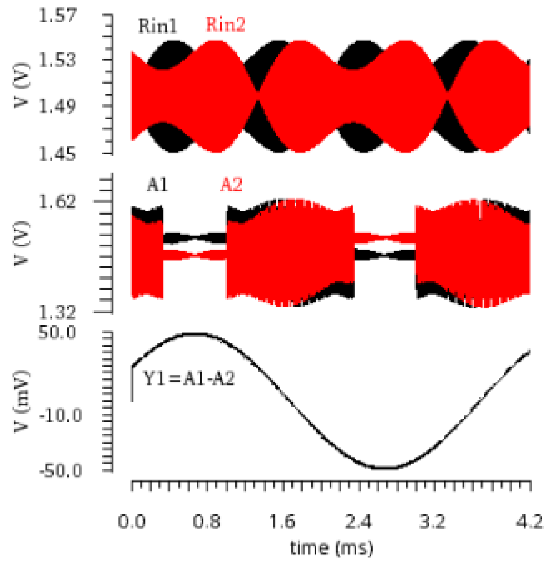

Fig. 12. Simulation results of $A_{1,2}$ and Y_1 within an envelope period.

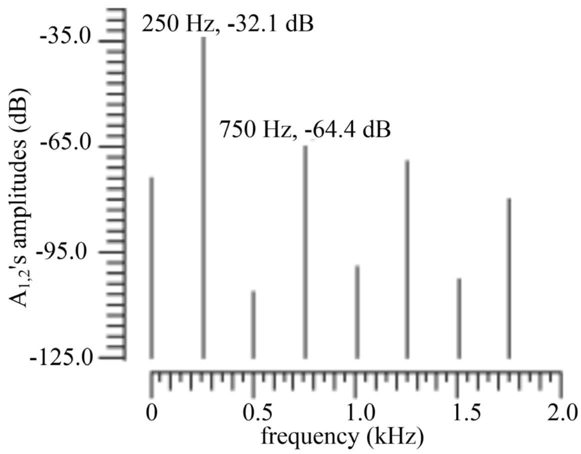

(a) $A_{1,2}$'s frequency spectrum

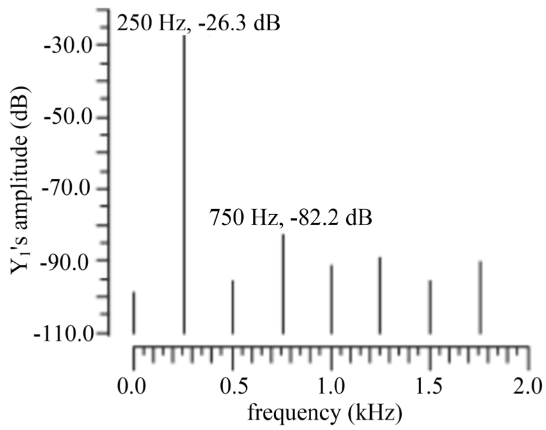

(b) Y_1's frequency spectrum

Fig. 13. Simulation results of frequency spectrum.

Works	Application	Active or passive	Digital or analog	Noise	Third harmonic
[5, 6, 8]	quadrature coils based	active	analog	large	large
[10]	three-phase coils based	—	—	—	large
[11]	three-phase coils based	active	analog	large	low
[17], [18]	—	active	analog	large	—
This work	three-phase coils based	passive	digital	low	low

Tab. 2. Comparisons of this work with the existing works.

5. Conclusions

A multi-channel differential synchronous demodulator is proposed for detecting envelope differences of every two of the induced voltages on three-phase receiving coils. Theoretical basis, circuits' design and simulation results are given and discussed in this work, in which the proposed circuits are realized in a 0.18 μm CMOS process and verified by Spectre simulator. Simulation results show the proposed demodulator works well, and third harmonics of the envelope differences of every two of the induced signals are much smaller than third harmonics of the envelope of the induced signals. These results indicate the proposed demodulator could be a candidate for realizing the high performance analog front-end of signal conditioning chip in three-phase receiving coils based linear IPS.

References

[1] SITTITHAI, P., PHAEBUA, K., LERTWIRIYAPRAPA, T., et al. Magnetic field shaping technique for HF-RFID and NFC systems. *Radioengineering,* 2019, vol. 28, no. 1, p. 121–128. DOI: 10.13164/re.2019.0121

[2] YOO, K., SEO, J., BAN, J., et al. Study on development of torque and angle sensor for EPS. *SAE International Journal of Passenger Cars - Electronic and Electrical Systems,* 2012, vol. 5, no. 1, p. 292–296. DOI: 10.4271/2012-01-0941

[3] ASCHENBRENNER, B., ZAGAR, B. G. Analysis and validation of a planar high-frequency contactless absolute position sensor. *IEEE Transactions on Instrumentation and Measurement*, 2015, vol. 64, no. 3, p. 768–775. DOI: 10.1109/TIM.2014.2348631

[4] KHALID, M. A., SALEEM, M. M., BUKHARI, S. A. R., et al. Design and characterization of three-axis high-range inductive tactile force sensor utilizing magnetorheological elastomer for robotic surgical. *IEEE Sensors Journal*, 2023, vol. 23, no. 1, p. 247–255. DOI: 10.1109/JSEN.2022.3222930

[5] RAHAL, M., DEMOSTHENOUS, A. An ASIC front end for planar high-frequency contactless inductive position sensors. *IEEE Transactions on Instrumentation and Measurement*, 2009, vol. 58, no. 9, p. 3021–3030. DOI: 10.1109/TIM.2009.2016819

[6] RAHAL, M., DEMOSTHENOUS, A. A synchronous chopping demodulator and implementation for high-frequency inductive position sensors. *IEEE Transactions on Instrumentation and Measurement*, 2009, vol. 58, no. 10, p. 3693–3701. DOI: 10.1109/TIM.2009.2019314

[7] RAHAL, M., DEMOSTHENOUS, A. An integrated signal conditioner for high-frequency inductive position sensors. *Measurement Science and Technology*, 2010, vol. 21, p. 1–12. DOI: 10.1088/0957-0233/21/1/ 015203

[8] ZOU, Y. T., ZHI, X. K., ZHANG, J., et al. A high accuracy lock-in transceiver for speed over 8000-r/min contactless eddy-current angular position sensors. *IEEE Transactions on Instrumentation and Measurement*, 2021, vol. 70, p. 1–12. DOI: 10.1109/TIM.2021.3101313

[9] HOBEIN, D., DORISSEN, T., DURKOPP, K. Progress in automotive position sensors and introduction of the Hella inductive position sensor. *SAE Technical Paper* 2004-01-1115, 2004. DOI: 10.4271/2004-01-1115

[10] ZHANG, C., LI, Z. P., CHEN, J., et al. Design and research of a novel non-contact vertical inductive torque sensor. *Measurement*, 2021, vol. 177, p. 1–10. DOI: 10.1016/j.measurement.2021.109252

[11] LUGANI, L., AKERMI, Y., LAVAL, P., et al. High speed inductive position sensor for E-machines. 7 pages. [Online] Available at: http:// media.melexis.com

[12] MATANGA, L. M. Performance evaluation and comparison of different inductive sensor-based position sensing approaches. *Master Thesis Report*. Grenoble INP-Phelma, Grenoble, 2021.

[13] BRAJON, B. Development of a hybrid magnetic-inductance angular sensor with 360° range and stray field immunity. *Master Thesis Report*. Politecnico Di Torino, Rome, 2020.

[14] MAK, P. I., U SENG PAN, MARTINS, R. P. On the design of a programmable-gain amplifier with built-in compact DC-offset cancellers for very low-voltage WLAN systems. *IEEE Transactions on Circuits and Systems-I: Regular Papers*, 2008, vol. 55, no. 2, p. 496–509. DOI: 10.1109/TCSI.2007.910643

[15] FATEMI-BEHBAHANI, E., FARSHIDI, E., ANSARI-ASL, K. Analysis of residue probability density function and comparator offset error in pipeilined ADCs. *Radioengineering*, 2016, vol. 25, no. 1, p. 208–215. DOI: 10.13164/re.2016.0208

[16] KIM, S. Y., ABBASIZADEH, H., ALI, I., et al. An inductive 2-D position detection IC with 99.8% accuracy for automotive EMR gear control system. *IEEE Transactions on Very Large Scale Integration Systems*, 2017, vol. 25, no. 5, p. 1731–1741. DOI: 10.1109/TVLSI.2017.2651112

[17] CASANELLA, R., CASAS, O., PALLÀS-ARENY, R. Differential synchronous demodulator for modulating sensors and impedance measurements. *Measurement Science and Technology*, 2005, vol. 16, p. 1637–1643. DOI: 10.1088/0957-0233/16/8/014

[18] GONZÁLEZ-LANDAETA, R., COTA-RUIZ, J., SIFUENTES, E., et al. A fully differential synchronous demodulator for AC signals.

IEEE Transactions on Instrumentation and Measurement, 2020, vol. 69, no. 1, p. 35–44. DOI: 10.1109/TIM. 2019.2895481

[19] MERZ, N., KIRANON, W., WONGTACHATHUM, C., et al. A modified bipolar translinear cell with improved linear range and its applications. *Radioengineering*, 2012, vol. 21, no. 2, p. 736 to 745. ISSN: 1210-2512

[20] ZHANG, S. F., ZHOU, X., GAO, C., et al. A 130-dB CMRR instrumentation amplifier with common-mode replication. *IEEE Journal of Solid-State Circuits*, 2022, vol. 57, no. 1, p. 278–289. DOI: 10.1109/JSSC.2021.3090100

[21] HU, C. Y., DATLINGER, C., ZHONG, Z. M., et al. Rotor position detection based on magnetically coupled resonant principle and its implementation. *IEEE Sensors Journal*, 2021, vol. 21, no. 6, p. 7402–7411. DOI: 10.1109/JSEN.2021.3050806

[22] YE, L., YANG, M., XU, L. Rotor study of inductive angle sensor. In *Int. Conf. on Mechatronics and Automation*. Chengdu (China), 2012, p. 697–701. DOI: 10.1109/ICMA.2012.6283227

About the Authors ...

Jun XUE was born in Wuhan City, Hubei province, China in 1985. He received his M.Sc. from Wuhan University in 2008. He is currently working in Wuhan Railway Vocational College of Technology, and his research interests include embedded system and angular sensors.

Dezhi WANG (corresponding author) was born in Jingzhou City, Hubei province, China in 1983. He received his Ph.D. degree from Huazhong University of Science and Technology in 2013. He is currently working in Hubei University and his research interests include high performance inductive position sensors and mixed-signal integrated circuits.